Methods for Event Reconstruction in the CBM Experiment

P.G. Akishin[1], E.P. Akishina[1], S.A. Baginyan[1], V.V. Ivanov[1], Val.V. Ivanov[1], I.V. Kisel[1,2], B.F. Kostenko[1], E.I. Litvinenko[3], G.A. Ososkov[1], A.M. Raportirenko[1], A.A. Soloviev[1], P.V. Zrelov[1], V.V. Uzhinsky[1]

[1] *Laboratory of Information Technologies, Joint Institute for Nuclear Research, 141980, Dubna, Russia*

[2] *Kirchhoff Institute of Physics, University of Heidelberg, 69120 Heidelberg, Germany*

[3] *Frank Laboratory of Neutron Physics, Joint Institute for Nuclear Research, 141980, Dubna, Russia*

Abstract

Methods and algorithms for event reconstruction in the CBM experiment are described. All these results have been developed and presented by the LIT team on CBM collaboration meetings in years 2004-2005.

The CBM Collaboration [1] builds a dedicated heavy-ion experiment to investigate the properties of highly compressed baryonic matter as it is produced in nucleus-nucleus collisions at the Facility for Antiproton and Ion Research (FAIR) in Darmstadt, Germany. The scientific goal of the research program of the CBM experiment is to explore the phase diagram of strongly interacting matter in the region of highest baryon densities. This approach is complementary to the activities at RHIC (Brookhaven) and ALICE (CERN-LHC) which concentrate on the region of high temperatures and very low net baryon densities.

The experimental setup has to fulfil the following requirements: identification of electrons which requires a pion suppression factor of the order of 10^5; identification of hadrons with large acceptance; determination of the primary and secondary vertices (accuracy $\sim 30\,\mu$m); high granularity of the detectors; fast detector response and read-out; very small detector dead time; high-speed trigger and data acquisition; radiation hard detectors and electronics; tolerance towards delta-electrons.

Fig. 1 depicts the present layout of the CBM experimental setup. Inside the dipole magnet gap are the target and a 7-planes Silicon Tracking System (STS) consisting of pixel and strip detectors. The Ring Imaging Cherenkov detector (RICH) has to detect electrons. The Transition Radiation Detector (TRD) arrays measure electrons with momentum above 1 GeV. The TOF stop detector consists of Resistive Plate Chambers (RPC). The Electromagnetic Calorimeter (ECAL) measures electrons, photons and muons. The CBM setup is optimized for heavy-ion collisions in the beam energy range from about 8 to 45 AGeV. The typical central Au+Au collision in the CBM experiment will produce up to 700 tracks in the inner tracker (see Fig. 2). Large track multiplicities together with the presence of a non-homogeneous magnetic field make the reconstruction of events extremely complicated. It comprises local track finding and fitting in the STS and TRD, ring finding in RICH, cluster reconstruction in ECAL, global matching between STS, RICH, TRD, TOF and ECAL, and the reconstruction of primary and secondary vertices.

Therefore the collaboration performs an extensive analysis of different track recognition methods in order to understand better the geometry of the detector and to investigate specific features of accepted events [1].

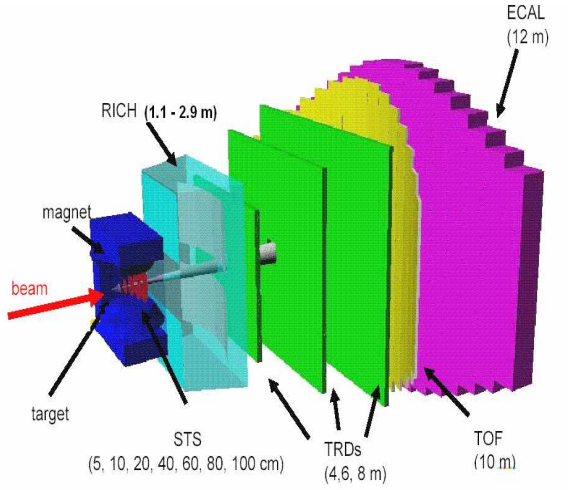

Fig.1. CBM general layout

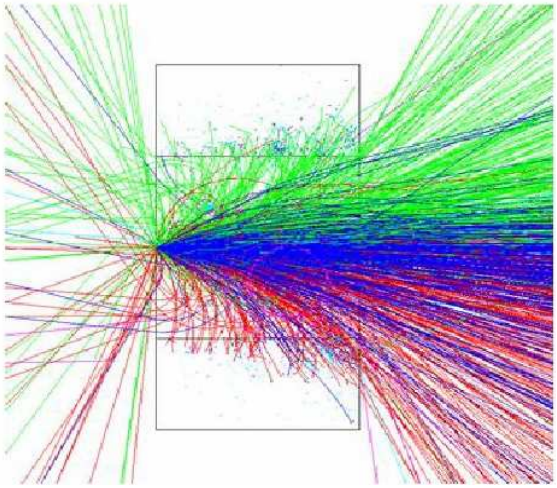

Fig.2. Visualization of a typical CBM event

1. The track reconstruction problem can be split into track finding and track fitting. Different competitive approaches to both track finding and the reconstruction of the initial track parameters were applied by the LIT specialists. For the track finding 3D track following and cellular automaton methods have been used. The Kalman filter and global fitting methods like the polynomial approximation are applied to the problem of momentum reconstruction. The Kalman filter was also used for the determination of the primary and secondary vertices.

1.1. 3D track-following method

The track-following method reconstructs tracks based on the hits measured in the STS tracking stations. The algorithm should be stable with respect to initial vertex coordinates and the STS geometry. We used some approaches known from [2]. The track recognition procedure is accomplished in 3D space on both x-z and y-z projections simultaneously. The procedure alternates between both views, predicting a track position on the next station and searching for hits in the vicinity of the predicted position. Starting from the middle of the target area, this point is sequentially connected with all hits in the first station in y-z view, where tracks are close to straight lines (see Fig. 3). The straight lines driven via these two points are prolonged to the plane of the second station. All hits in an asymmetrical corridor around the intersection point are then used for fitting a parabola in x-z view which is prolonged to the next station. Since several prolongations can happen, we set aside corridors around each point predicted on the third station. A similar corridor is set in the y-z view on the third station. If hits are found in those limits, they are attached to the track. The method continues the track prolongation and searching for hits in corridors around the predicted position towards the outer stations. Each new parabolic prolongation is done with the corresponding curvature radius r calculated **taking the magnetic field into account** (see Fig. 4). The high accuracy predictor is based on special tables with confidence bounds of prediction corridors. These tables are calculated preliminary on the basis of the distributions of deviations between real hit

positions and their predictions. Calculations have to be done by Monte-Carlo simulations of a considered sample of heavy-ion events in the STS for all stations.

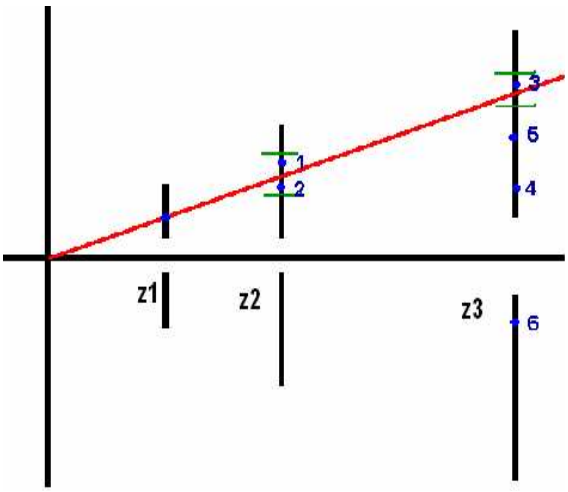

Fig.3. Prediction and search in YoZ view

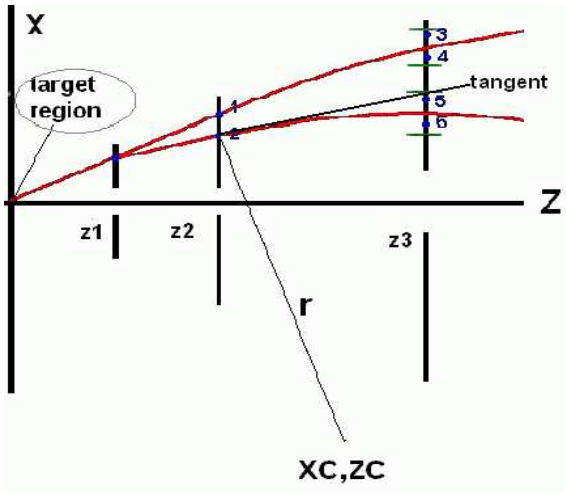

Fig.4. Prediction and search in YoZ view taking into account the local track curvature

On the data simulated for the initial STS deign based on hybrid pixel stations, 3D track following approach has shown quite a satisfactory efficiency on the level 92-96% and a very low level of ghost tracks, but for the most recent STS design with the first three stations constructed on the MAPS technology and the other 4 stations based on silicon strip wafers its efficiency felt down drastically demanding a more elaborated predictor.

Much better results were obtained by the second track reconstruction procedure based on a combination of a cellular automaton application for track-element recognitions and Kalman filter as a predictor.

1.2. Cellular Automaton based track finding

The cellular automaton method [3, 4] creates short track segments (tracklets) in neighbouring detector planes and strings them into tracks (see Fig. 5). Being essentially local and parallel, cellular automata avoid exhaustive combinatorial searches, even when implemented on conventional computers. Since cellular automata operate with highly structured information, the amount of data to be processed in the course of the track search is significantly reduced. As a rule, cellular automata employ a very simple track model which leads to utmost computational simplicity and a fast algorithm. By definition, the reconstructed track is assigned to a generated particle, if at least 70% of its hits have been caused by this particle. A generated particle is regarded as found, if it has been assigned to at least one reconstructed track. If the particle is found more than once, all additionally reconstructed tracks are regarded as clones. The reconstructed track is called a ghost, if it is not assigned to any generated particle (70% criteria). The efficiency of track reconstruction for particles detected in at least four stations is presented in Fig. 6. Tracks of high momentum particles are reconstructed very well with efficiencies of 99.45%, while multiple scattering in detector material leads to a lower reconstruction efficiency of 89.46% for slow particles. The reconstruction efficiency for fast primary tracks with momentum higher than 1 GeV/c is almost 100%, while the efficiency of all fast tracks is slightly lower because of the presence of secondary tracks, originating far downstream from the target region. The total efficiency for all tracks with a large fraction of soft

secondary tracks is 96.98%. The clone rate is not a problem for the algorithm (0.01%). the ghost level is at 0.61%.

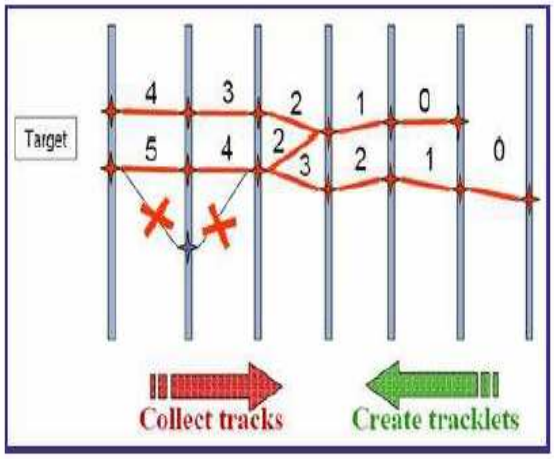

Fig.5. A simple illustration of the cellular automaton algorithm. It creates tracklets, links and numbers them as possibly situated on the same trajectory, and collects tracklets into track candidates

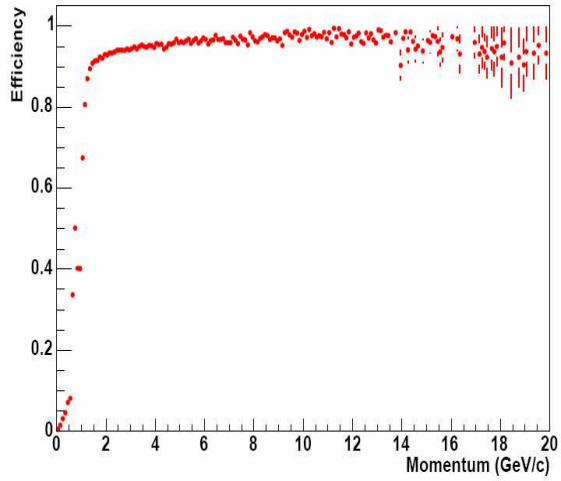

Fig.6. Track reconstruction efficiency as a function of momentum

2. Track and vertex fitting have been done using the Kalman filter based procedures [1, 6]. Propagation of tracks in non-homogeneous magnetic field is based on a specially developed analytic formula [7, 8]. Mean relative momentum resolution for all tracks is 0.69%. Secondary tracks from D^0 decay being longer have slightly better momentum resolution of 0.67%. After the primary vertex is reconstructed, tracks identified as primary can be refitted with an additional constraint to the primary vertex position. This improves their average track momentum resolution to 0.63%.

The **primary vertex** was determined from all tracks reconstructed in the STS excluding those which formed well detached vertices like K^0_S and Λ decays. The Kalman filter based algorithm reconstructs the primary vertex with the accuracy of 4 μm for the longitudinal and better than 1 μm for transversal components of the primary vertex position.

Precision of the **secondary vertex** parameters obtained in the geometrical vertex fit can be improved by taking into account several assumptions on tracks associated to the vertex. Two types of constraints have been included into the secondary vertex fit: a mass constraint and a topological constraint. The mass constraint is usually applied in the case of one or several combinations of particles in the vertex are known to originate from a narrow width mass state. The topological constraint is used to point a mother particle to the (already reconstructed) primary vertex. The final accuracy is 44.4 μm for the longitudinal and 1.7 μm for transversal components of the secondary vertex position for D^0 decay.

3. Momentum estimation has been realized by two approaches: polynomial approximations and orthogonal polynomial sets.

3.1. Polynomial approximations

This algorithm reconstructs the particle momentum directly from the hits in the Silicon

Tracking System (STS). It consists of two steps. First, the track curve is fitted by a polynomial vector function, using the smoothness of the trajectory. Three types of approximation were applied: polynomials, cubic splines and B-splines. The optimisation problem is described by the residual function

$$F = \sum_{i=0}^{N} \left[\left(\frac{\hat{x}(z_i) - x_i}{\sigma_x^i} \right)^2 + \left(\frac{\hat{y}(z_i) - y_i}{\sigma_y^i} \right)^2 \right],$$

where x_i, y_i are the trajectory hits, $\hat{x}(z)$, $\hat{y}(z)$ the coordinate approximations, σ_x^i, σ_y^i are the measurement errors, and N – the number of hits in the tracking system. It should be noted that F is a quadratic functional of the parameters describing the coordinate functions $\hat{x}(z)$, $\hat{y}(z)$. This means that the optimization problem is reduced to a very fast procedure of multiplication of an a priory prepared matrix with the vectors of hit coordinates.

In the second step, the constructed functions $\hat{x}(z)$, $\hat{y}(z)$ are used to determine the approximate value of the momentum. The momentum reconstruction is based on the equations of motion:

$$x_{zz} = \frac{kq(1 + x_z^2 + y_z^2)^{\frac{1}{2}}}{p} \{x_z y_z B_x - (1 + x_z^2) B_y + y_z B_z\},$$

$$y_{zz} = \frac{kq(1 + x_z^2 + y_z^2)^{\frac{1}{2}}}{p} \{(1 + y_z^2) B_x - x_z y_z B_y - x_z B_z\},$$

where p and q are momentum and charge of the particle, respectively, and B_x, B_y, B_z the components of the nonuniform magnetic field in the point (x, y, z); x_z, y_z and x_{zz}, y_{zz} denote the first and second derivatives of x and y with respect to z, respectively. With the density function

$$f(\alpha, z, \hat{x}(z), \hat{y}(z)) = |x_{zz} - \alpha kq(1 + x_z^2 + y_z^2)\{x_z y_z B_x - (1 + x_z^2) B_y + y_z B_z\}|^2 +$$

$$+ |y_{zz} - \alpha kq(1 + x_z^2 + y_z^2)^{\frac{1}{2}} \{(1 + y_z^2) B_x - x_z y_z B_y - x_z B_z\}|^2$$

the approximated value p is derived as the inverse of minimising functional

$$G(\alpha) = \int_{z_b}^{z_e} f(\alpha, z, \hat{x}(z), \hat{y}(z)) g(z) dz,$$

where $g(z)$ is a weight function and z_b, z_e are the z coordinates of the first and last STS detector, respectively. Since $G(\alpha)$ is a quadratic functional of the parameter α, a fast non-iterative procedure for the evaluation of p can be constructed.

This algorithm has been applied to simulated tracks in the momentum range 1 - 10 GeV/c with hits in all seven stations of the STS. Ideal track finding was assumed. The first and second momenta of the relative momentum residual distributions are summarized in Table 1. While in the absence of multiple scattering (MS), the spline approximations give better results, the performance in the presence of multiple scattering is similar for all three approximations (σ_p = 0.75-0.80 %).

3.2. Orthogonal polynomial sets

The method of accurate momentum reconstruction with orthogonal polynomial sets constructs an explicit function which gives the momentum in terms of measurable quantities:

Table 1: Mean and RMS of the momentum residual distributions

Track model	$<\frac{\Delta p}{p}>$ [%] no MS	$<\frac{\sigma_p}{p}>$ [%] no MS	$<\frac{\Delta p}{p}>$ [%] MS	$<\frac{\sigma_p}{p}>$ [%] MS
polynomial	-0.02	0.28	-0.02	0.76
cubic spline	0.08	0.17	0.09	0.79
B spline	0.01	0.16	0.00	0.78

position and direction of a track at the entrance of the spectrometric field and the deflection angle as the effect of the field onto the track momentum [9]-[11]. This experimental input information can be provided e. g. by a Kalman filter operating on hits registered in the CBM silicon tracking system (STS).

In inhomogeneous magnetic field φ is a function of p, position and direction of a charged particle at the magnet entrance

$$\varphi = \varphi(X_1, Y_1, A_x, A_y, p), \tag{1}$$

(X_1, Y_1, Z_1) is the point in the first STS, (A_x, A_y) are the tangents of the particle trajectory in this point. The task is to construct the inverse function

$$p = p(X_1, Y_1, A_x, A_y, \varphi), \tag{2}$$

which provides accurate momenta restoration [11].

The procedure consists of two steps:

1. The deflection angles for the given magnetic field are calculated for a set of representative trajectories.

2. The explicit function (2) is then constructed on the basis of these trajectories.

Each trajectory is defined by five variables:

1. $(x_1 = X_1,\ y_1 = Y_1)$ - coordinates of a point in the first STS;

2. $(x_3 = A_x,\ x_4 = A_y)$ - tangents of a particle trajectory in the point (X_1, Y_1);

3. $x_5 = 1/(p \cdot c)$, p is the particle momentum, c - speed of light.

Let $[A_i, B_i]$ be the range of i-th variable: $i = 1, 2, ..., 5$. Each variable is normalized to the range [-1, +1]

$$g_i = \frac{2x_i - A_i - B_i}{B_i - A_i} \tag{3}$$

and a discrete number of *"nodes"*, according to the Tchebycheff distribution

$$g_i = g_i(\alpha_i) = \cos\frac{(2\alpha_i - 1)\pi}{2N_i}, \quad \alpha_i = 1, ..., N_i, \quad i = 1, ..., 5,$$

is chosen. The set of $N_1, N_2, ..., N_5$ determines the collection of fixed trajectories, which are traced through the magnetic field, and the set of corresponding deflections $\varphi(x_1, x_2, x_3, x_4, x_5)$ is calculated.

Let the range of $\varphi(\cdot)$ be $[A_6, B_6]$; $\varphi(\cdot)$ is also normalized to the range [-1, +1]:

$$g_6 = \frac{2\varphi - A_6 - B_6}{B_6 - A_6}$$

and a discrete number of values g_6

$$g_6 = g(\alpha_6) = \cos\frac{(2\alpha_6 - 1)\pi}{2N_6}, \quad \alpha_6 = 1, ..., N_6, \quad N_6 \leq N_5$$

is chosen. Now, applying the inverse interpolation, we can calculate the corresponding values of g_5.

Let g_5 be in the form

$$g_5 = \sum_{ijklm} C_{ijklm} T_i(g_1) T_j(g_2) T_k(g_3) T_l(g_4) T_m(g_6), \tag{4}$$

$i = 0, ..., N_1 - 1$; $j = 0, ..., N_2 - 1$; $k = 0, ..., N_3 - 1$; $k = 0, ..., N_4 - 1$; $m = 0, ..., N_6 - 1$. The coefficients C_{ijklm} are calculated using the formula:

$$C_{ijklm} = \frac{\sum\limits_{\alpha_1\alpha_2\alpha_3\alpha_4\alpha_6} g_{5_{\alpha_1\alpha_2\alpha_3\alpha_4\alpha_6}} T_i(g_1) T_j(g_2) T_k(g_3) T_l(g_4) T_m(g_6)}{(\sum\limits_{\alpha_1} T_i(g_1))^2 (\sum\limits_{\alpha_2} T_j(g_2))^2 (\sum\limits_{\alpha_3} T_k(g_3))^2 (\sum\limits_{\alpha_4} T_l(g_4))^2 (\sum\limits_{\alpha_6} T_m(g_6))^2}, \tag{5}$$

$\alpha_1 = 1, ..., N_1; \alpha_2 = 1, ..., N_2; \alpha_3 = 1, ..., N_3; \alpha_4 = 1, ..., N_4; \alpha_6 = 1, ..., N_6$.

The total number of *"nodes"* for which trajectories were calculated was 625: $N_1 = N_2 = N_3 = N_4 = 5$. The trajectories were computed for each sample and for $N_5 = 7$ momentum values in the range 1-10 GeV/c and the deflection angle was determined. For each combination $(\alpha_1, \alpha_2, \alpha_3, \alpha_4)$ the momentum variable was calculated by inverse interpolation for $N_6 = 7$ of deflection variables. Then, using (5), the expansion coefficients C_{ijklm} were calculated: total number is 5 x 5 x 5 x 5 x 7 = 4375. Lowering the upper limits N_1, N_2, N_3, N_4, N_6, we obtain, without changing the coefficients, a least-squares fit to the computed trajectories. This is a consequence of the Tchebysheff polynomials being orthogonal. The number and significant coefficients can be found by a Fisher test. Our analysis has shown that without loss in accuracy, only 89 coefficients can be used. In order to estimate the accuracy of the method on data close to real data, we used the GEANT data. Fig. 7 presents the distribution of $p - p_c$ and Fig. 8 shows the distribution of $\frac{p-p_c}{p}$ for positively charged tracks. One can see from Fig. 4 that the dispersion of the distribution $\frac{p-p_c}{p}$ is 0.26%.

It must be noted that this result is obtained for positively charged particles, because the tracing of the basic set of trajectories was realized for positively charged particles. For a small part of tracks ($\approx 10\%$), the parameters of which are out of the range of variables x_1, x_2, x_3, x_4, x_6, we used the approximation of the uniform magnetic field. This reduces the overal resolution to about 0.34%.

In summary, the algorithm provides the possibility to reconstruct the momentum of charged particles registered in the STS system with high accuracy. The accuracy can be further improved by separate momentum reconstruction of particles of different charges and by subdivision of the momentum range into subintervals.

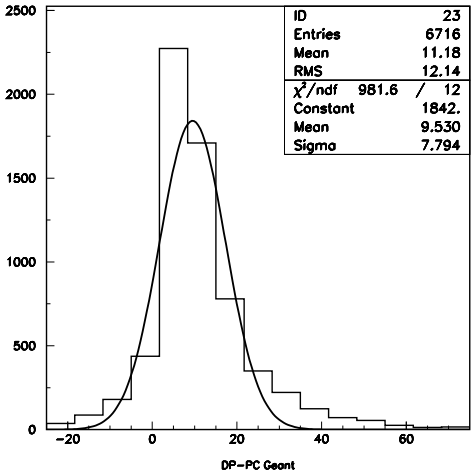

Fig. 7. Distribution of $p - p_c$ (in MeV/c) for the GEANT data (for positively charged particles)

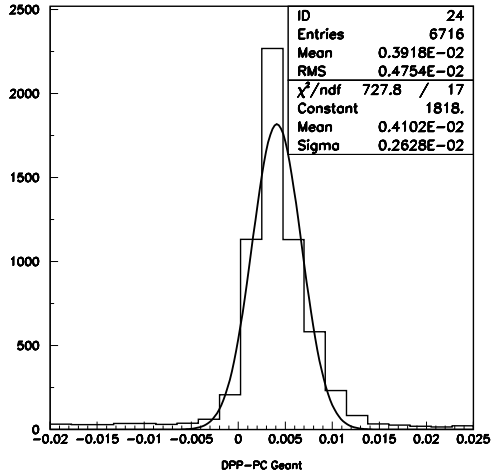

Fig. 8. Distribution of $\frac{p-p_c}{p}$ for the GEANT data (for positively charged particles)

4. Particle identification with the RICH detector

The Ring Imaging Cherenkov detector (RICH) is designed to provide electron identification in the momentum range of electrons from low-mass vector-meson decays. A second task of the RICH detector is the p identification for higher momenta in order to improve the K/p separation which quickly deteriorates for $p > 4$ GeV/c if only time-of-flight information is used. Particle identification with the RICH detector is performed by a measurement of the Cherenkov angle/ring radius and the momentum of the particles (see Fig. 10). Assuming that tracks with momentum are provided by the tracking system, the RICH part for particle identification requires the following steps:

- ring finding,
- determination of center and radius of ring/ Cherenkov angle,
- matching of rings with tracks.

All charged tracks being reconstructed by the tracking system are reflected at the mirror in order to give the center of a possible Cherenkov ring (see Fig. 9). The number of these tracks is much larger than the number of particles really producing a ring. In order to combine rings and tracks each ring is to be matched to the track having its extrapolation closest to the calculated ring center.

Track extrapolation was obtained using CbmRichProjectionProducer class. Each RICH event consists of about 400 track extrapolations and about 1500 hits, nearly 80 rings. So the key part of any ring-finder is a prior search for all ring containing fragments. It was realized by the coarse histogramming of source data, then by clustering hits in all separate areas of this histogram and by choosing not all, but only hits belonging to each of those clusters.

Methods for CBM-RICH ring recognition were elaborated on the basis of the fast search for the areas containing RICH hits and then either by using the information of previously found tracks or, as a standalone program, for unguided ring finding.

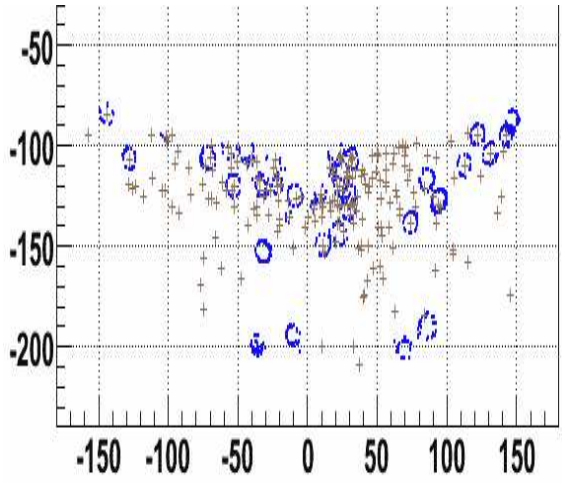

Fig.9. Simulated image of the CBM RICH photodetector plane. Hits forming rings to be recognized are marked by blue points. Track prolongations to this plane are marked by crosses

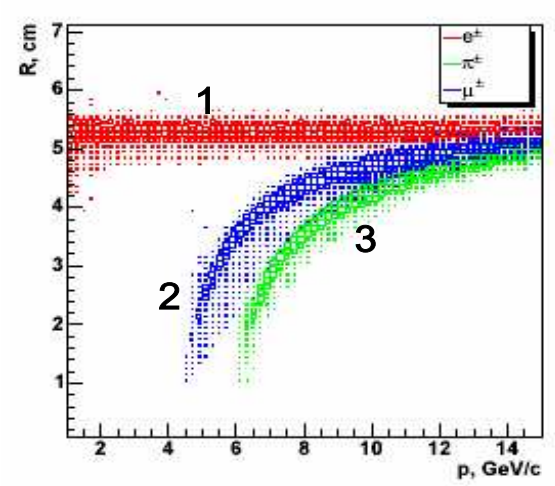

Fig.10. Ring radius distribution versus the track momentum for $e^{\pm}$ (1), $\mu^{\pm}$ (2) and $p^{\pm}$ (3)

4.1. Track based RICH-ring recognition algorithm

Each track extrapolation could be considered as a potential ring center. However, as it can be seen from Fig. 9, the high multiplicity of CBM events, especially the great number of secondary particles cause the track-ring matching problem. It is solved by combining track and ring with closest distance. We calculate all distances between ring center predicted by track and nearest hits. Each time we test these distances to be within prescribed limits. Then we histogram those distances and look for a maximum. If the sum of maximum bin and of two adjacen bins is exceeded a CUT, that means that we found a ring. Natural criteria were aslo applied:

1. Δr = difference of fitted radius and simulated radius < 0.5 cm;
2. Δxy = difference of fitted ring center and simulated center < 0.5 cm;
3. min/max potential hits (compare MC hits and associated hits) in the range 0.5 - 1.5.

The total efficiency of track-guided ring finding shown in Figs. 11 and 12 is on the satisfactory level.

Since we use the track extrapolation as a ring finding predictor, we have ring finding and track-ring matching in one. But if we have two very close tracks, a mismatching problem arises (see Fig. 13). Fortunately, as it is seen in Figs. 14 and 15, mismatching errors are on the level less than 10%, although such a circle of problems needs to be better studied.

The second approach to the **unguided ring recognition** leading to the so-called **standalone ring-finding** is of importance for various problems of the RICH instrumental testing and of the RICH alingnment with other detectors of the CBM setup. There were three independent methods proposed: Hough transform based, moving templates and elastic networks approaches.

4.2. The Hough Transform approach was studied as an option for a standalone ring

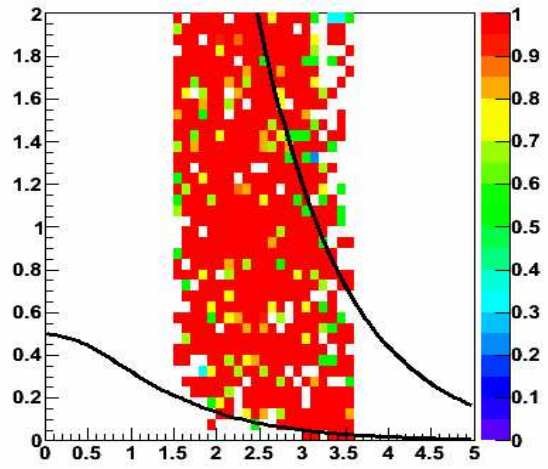

Fig.11. Ring-finding efficiency for electrons as the function of Pt (GeV/c) (vertical axis) and rapidity

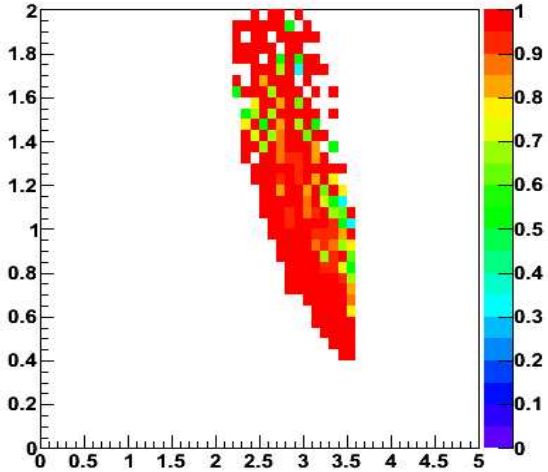

Fig.12. Ring-finding efficiency for pions as the function of Pt (GeV/c) (vertical axis) and rapidity

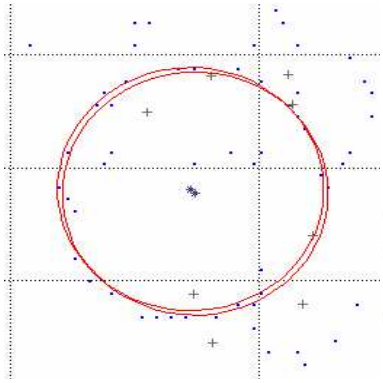

Fig.13. Two tracks one ring

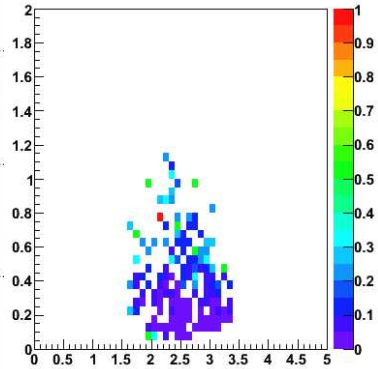

Fig.14. Wrong matches: real rings

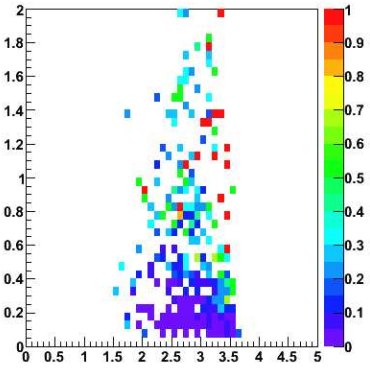

Fig.15. Matching of fake rings

finder providing center and radius for each ring. It can as well be used to give an estimate of center and radius of the rings which then can be used as input for fitting the ring . The Hough transform framework is often applied to cope with low resolution search of rings. The Hough transform is robust to a certain extent concerning topological gaps in rings (semicircles at detector edges) and concerning a high noise background [13, 14]. It converts points of the measurement space, i.e. hits, to points in the parameter space. In case of circles in the RICH detector the coordinates of the parameter space are the ring centers and their radii. Through three arbitrary signal points a unique circle can be drawn. The resulting ring centers show a wide distribution in the parameter space and nearly fill the full circle of real rings. This effect can easily be understood considering the fact, that the ring center and the radius from the neighboring hits are only vaguely determined. Unfortunately, heavy combinatorics inherented to any Hough transform implementation results in its very high time consuming. Therefore, a procedure was developed reducing the number of combinations. In the next step of the usual Hough transform strategy, ring centers and radii are determined by the search for the most populated places in the parameter space. A simple method would consist of collecting all calculated centers (xc,yc) in histograms of proper granularity and defining a cut-off value in the signal height to

select real ring centers. The radii corresponding to each center can then be found similarly.

4.3. Moving template (MT) approach to ring search

A template (a blue area in Fig. 16) was elaborated to cover only electron rings, $r \approx 5.5 \pm 0.5$ cm, even elliptically and stochastically deformed. The ring is "caught" by matching its left hits with the left edge of the template. The ring is recognized using its characteristic features (qualitative and quantitative) by examination of a picture which hits form within the template region. Found rings are marked out (by red in the picture). This approach could be applicable to handle cases of "spoiled" rings due to spherical aberration or the stray magnetic field.

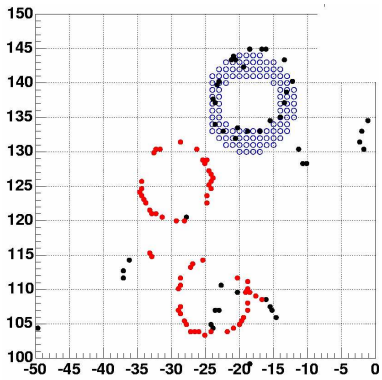

Fig.16. Moving template example

4.4. Elastic Net for standalone RICH ring finding

Standalone finding of rings in RICH detector is based on the elastic neural net [16, 17]. The method does not require any prior track information and can be used for triggering. Application of the method to the RICH detector of the CBM experiment shows an efficiency of 94.3% and high speed (5.4 ms per event with about 1400 hits in the RICH detector). In view of its computational simplicity and high speed, the algorithm is considered to be further implemented in hardware which can increase the speed by another few orders of magnitude.

4.5. The ring fitting

This algorithm was implemented as the program RFit which embodied the least squares algorithm (LSF) for estimating parameters of Cherenkov rings over a set of scattered points provided by the RICH detector. Since the conventional LSF is often failed for highly contaminated data, it was evolved to the robust weighted LSF [12]. The RFit program supports both algorithms for fitting a single ring and even two overlapped rings simultaneously (see [15] for the algorithm description). It was carefully tested on the big sample of simulated events and showed the satisfactory accuracy and efficiency.

5. Algorithms for STS and TRD tracking

These algorithms were developed as track following in space on the basis of the Kalman filter taking into account both the nonlinear magnetic field and the multiple scattering. The track following process is an originated downstream beam from the middle of the target area, but then after finding several reference tracks with momentum over 5 GeV it can estimate and use the approximate vertex position. The program was tested on the GEANT simulated STS and TRD data, but needs its further tuning.

References

[1] Compressed Baryonic Matter Experiment. Technical Status Report, GSI, Darmstadt, 2005 (http://www.gsi.de/onTEAM/dokumente/public/DOC-2005-Feb-447 e.html).

[2] G.A. Ososkov, A. Polanski, I.V. Puzynin, Modern Methods of Experimental Data Processing in High Energy Physics, PEPAN, v.33, p.3, (2002), 676-745.

[3] I. Kisel, Fast tracking in the CBM experiment, 11th Workshop on Electronics for LHC and future Experiments (LECC2005), 12-16 September, 2005, Heidelberg, Germany.

[4] I. Kisel, Tracking in the CBM experiment, Workshop on Tracking in High Multiplicity Environments (TIME05), 03-07 October, 2005, Zurich, Switzerland (to appear in Nucl. Instr. and Meth. A).

[5] R. Arnold, C. Augier, A.M. Bakalyarov, . . . , I.Kisel at al. (NEMO Collaboration), Technical design and performance of the NEMO 3 detector, Nucl. Instr. and Meth. A 536 (2005) 79-122.

[6] S. Gorbunov, I. Kisel and Iou. Vassiliev, Analysis of D0 meson detection in Au+Au collisions at 25 AGeV, CBM note CBM-PHYS-note-2005-001, 23 June 2005.

[7] S. Gorbunov and I. Kisel, An analytic formula for track extrapolation in an inhomogeneous magnetic field, CBM note CBM-SOFT-note-2005-001, 18 March 2005.

[8] S. Gorbunov and I. Kisel, Analytic formula for track extrapolation in non-homogeneous magnetic field, X International Workshop on Advanced Computing and Analysis Techniques in Physics Research (ACAT 2005), May 22-27, 2005, DESY, Zeuthen, Germany (to appear in Nucl. Instr. and Meth. A).

[9] C. Lechanoine, M. Martin and H. Wind, Nucl. Inst. and Meth. 69 (1969) 122-124.

[10] L.S. Azhgirey et al., Measurements of the magnetic map of the spectrometric magnet SP12A, Communication of JINR, 13-86-164, Dubna, 1986 (in Russian).

[11] A.Yu. Bonushkina and V.V. Ivanov, Momenta restoration of charged particles detected by the MASPIK spectrometer, Communication of JINR, P10-93-125, Dubna, 1993 (in Russian).

[12] H.Agakishiev, O.Barannikova, F.Ceretto, U.Faschingbauer, P.Glassel, E.Kolganova, G.Ososkov, Yu.Panebratsev, J.Rak, N.Saveljic, I.Tserruya, T.Ullrich, J.P.Wurm, New Robust Fitting Algoritm For Vertex Reconstruction in the CERES Experiment, Nucl. Instr. and Methods A394 (1997) 225-231.

[13] L. Muresan, R. Muresan, G.Ososkov, Yu. Panebratsev, Deformable Templates for Circle Recognition, JINR Rapid Comm. 1[81]-97, 27-44.

[14] Baginyan, S., Ososkov, G., Finding tracks detected by a drift tube system, CPC, v 108 (1998) 20-28.

[15] G.Ososkov, Novel approch in RICH data handling, Czech. J. Phys. Vol.49/S2 (1999) 145-160.

[16] S. Gorbunov and I. Kisel, Elastic net for standalone RICH ring finding, CBM note CBM-SOFT-note-2005-002, 22 September 2005.

[17] S. Gorbunov and I. Kisel, Elastic net for standalone RICH ring finding, X International Workshop on Advanced Computing and Analysis Techniques in Physics Research (ACAT 2005), May 22-27, 2005, DESY, Zeuthen, Germany (to appear in Nucl. Instr. and Meth.A).